Hindawi
International Transactions on Electrical Energy Systems
Volume 2024, Article ID 9378284, 13 pages
https://doi.org/10.1155/2024/9378284

*Research Article*

# Design of PMSM Dual-Loop Control Systems Integrating LADRC and PI Controllers via an Improved PSO Algorithm

**Baoye Song**,[1] **Ruoyu Wang**,[1] **and Lin Xu**[2]

[1]*College of Electrical Engineering and Automation, Shandong University of Science and Technology, Qingdao 266590, China*
[2]*College of Energy and Mining Engineering, Shandong University of Science and Technology, Qingdao 266590, China*

Correspondence should be addressed to Baoye Song; songbaoye@sdust.edu.cn

Received 19 October 2023; Revised 22 December 2023; Accepted 28 December 2023; Published 5 January 2024

Academic Editor: Arvind R. Singh



This paper is concerned with the design of a dual-loop control system for permanent magnet synchronous motor (PMSM). An improved linear extended state observer (LESO) with excellent estimation capability is employed to develop an improved linear active disturbance rejection control (LADRC) suitable for PMSM speed regulation, achieving outstanding disturbance suppression in PMSM speed control. The use of an internal model control scheme to initialize the parameters of the proportional-integral- (PI-) based current controller simplifies the search space of the control system parameter optimization. An improved particle swarm optimization (PSO) algorithm is applied to optimize the controller parameters, thereby enhancing the overall system performance. Finally, through a series of simulations and experiments, we validate that our proposed controller exhibits superior performance compared to some other control methods.

## 1. Introduction

The permanent magnet synchronous motor (PMSM) is a type of electric motor that uses permanent magnets to create a magnetic field and achieve synchronous rotation. Owing to the advantages of high efficiency, compact size, high power density, and excellent dynamic response, PMSMs have been widely used in various applications [1, 2], including industrial machinery, electric vehicles, robotics, and renewable energy systems.

In practical engineering, proportional-integral-derivative (PID) control is the most common control technique used for regulating the speed or position of a servo PMSM, but it still has some deficiencies, e.g., limited robustness to parameter variations, restrictions in disturbance rejection, and difficulties in controller tuning, which would limit its performance in many applications [3, 4]. To address the aforementioned problems, many control schemes have been employed to enhance the performance of PMSM control systems in recent years, e.g., optimal control [5], adaptive control [6], model predictive control [7], internal model control [8], and sliding mode control [9]. Although the abovementioned control methods can improve the performance of PMSM servo systems, they still struggle to deal with some of the inadequacies [10–12], such as the instability caused by oscillation in the control system, the need for accurate model information in the controller design, and the presence of internal and external uncertain disturbances, among others.

To handle the problems mentioned above, active disturbance rejection control (ADRC), which does not require an accurate system model [13, 14], has attracted many researchers to devote their attention to the disturbance-tolerant control of PMSMs [15, 16]. For example, a nonlinear multi-input multi-output algorithm based on ADRC has been developed for the decoupled vector control of PMSMs [17]. The simulation results can verify the algorithm's improved static and dynamic performance. In [18], a hybrid algorithm combining sliding mode control and ADRC has been developed to promote the disturbance-rejection ability as well as the static and dynamic speed-tracking performance of PMSMs. In [19], the nonlinear ADRC has been utilized for the control of PMSMs, which exhibits significant improvements in robustness and disturbance-rejection capabilities in comparison with the traditional proportional-integral (PI) control. In [20], the extended state observer (ESO) of the nonlinear ADRC has been employed for estimating and compensating for the total disturbance of the system, thereby achieving the disturbance-tolerant decoupling control of PMSMs, which can expand the speed regulation range and enhance the precision of the controller. Though ADRC is model independent and offers strong disturbance-rejection capabilities, it has to face the challenge of tuning many control parameters, making it unfavorable in real applications.

To promote the practical application of ADRC in engineering, the linear active disturbance rejection control (LADRC) has been proposed in [21], which replaces the nonlinear part of the ADRC controller with linear functions and establishes a relationship between the controller's parameter and desired bandwidth. LADRC can reduce the number of parameters to regulate and make the tuning of parameters easier to implement [22, 23]. Although LADRC has shown its advantages in control systems, to the best of our knowledge, only regular methods have been applied and little effort has been made to enhance the observation ability of the linear extended state observer (LESO), which is one of the core functional modules of LADRC. As such, in this paper, we are motivated to challenge the design problem of LADRC based on an improved LESO (ILESO) for the PMSM control system, thereby further improving the control performance by accurately estimating the internal and external disturbances of the system.

Furthermore, PMSM control systems typically adopt dual-loop controllers for the speed and current regulation of PMSMs, which have many parameters to optimize. As such, the parameter tuning of the control system is a time-consuming and labor-intensive task for researchers. To cope with this intractable issue, extensive research efforts have been focused on exploiting heuristic algorithms to alleviate the burden of the tedious task, e.g., the particle swarm optimization (PSO) algorithm [24], genetic algorithm (GA) [25], pigeon-inspired optimization (PIO) algorithm [26], and differential evolution (DE) algorithm [27]. Despite the considerable research efforts, it is still a complex task to develop a reliable heuristic algorithm with strong capabilities to avoid premature convergence and escape from local optima, and this problem constitutes another motivation for the current study.

Motivated by the abovementioned discussions, this paper focuses on exploring the design of PMSM control systems integrating LADRC and PI controllers via an improved PSO algorithm. To design the speed controller for PMSMs, a modified LADRC (MLADRC) approach is employed, incorporating an improved LESO methodology. Subsequently, the PI controller for the current control of PMSMs is devised by initializing the controller parameters through the internal model scheme. Furthermore, the parameters of the speed and current controllers are fine-tuned using an improved PSO algorithm simultaneously. Finally, the effectiveness and superiority of the proposed methodology are validated through a series of simulations and experiments.

The main contributions of this paper can be summarized as follows:

(1) Using an improved LESO as a foundation, we introduce a modified LADRC system for superior disturbance rejection in PMSM speed control.

(2) For the current control of PMSMs, PI controllers are devised with their parameters initialized through the internal model scheme.

(3) To optimize both the speed and current controllers within the PMSM control system, an improved PSO algorithm is employed to tune the parameters of the whole system simultaneously.

(4) Through a series of simulations and experiments, we validate the superior performance of our proposed controller in comparison to other control methods.

The remainder of this paper is arranged as follows. Section 2 provides an overview of the preliminaries, covering the mathematical model and vector control of PMSMs. In Section 3, the design of the speed controller for PMSMs is discussed, focusing on the utilization of a modified LADRC approach. Section 4 is dedicated to explaining the design of the PI controller for the current control of PMSMs. Section 5 introduces an improved PSO algorithm employed for tuning the parameters of the control system. The results of simulations and experiments are reported in Section 6. Finally, Section 7 concludes the paper and outlines future research directions.

## 2. Preliminaries

*2.1. Mathematical Model of PMSMs.* The mathematical model of PMSMs is usually established based on the following assumptions [28]:

(1) The saturation of the motor's core can be ignored.

(2) The eddy current and hysteresis losses of the motor can be neglected.

(3) The current of the motor is in the ideal sinusoidal waveform.

Keeping the abovementioned assumptions in mind, the mathematical model of PMSMs in the $d$-$q$ reference frame can be described by the following equations [29].

The voltage equations of PMSMs can be expressed as follows:

$$\begin{cases} u_d = Ri_d - \omega_e L_q i_q + L_d \dfrac{di_d}{dt}, \\ u_q = Ri_q + \omega_e\left(L_d i_d + \psi_f\right) + L_q \dfrac{di_q}{dt}, \end{cases} \tag{1}$$

where $u_d$ and $u_q$ represent the voltage components in $d$-$q$ axes, respectively; $i_d$ and $i_q$ indicate, respectively, the current components in $d$-$q$ axes; $L_d$ and $L_q$ are the corresponding inductance components; $R$ denotes the stator resistance of the motor; $\omega_e$ denotes the electrical angular velocity of the motor; and $\psi_f$ stands for the flux linkage of the rotor magnet. It should be noted that the time $t$ of the variables is omitted in this paper, unless otherwise specified.

The electromagnetic torque equation of PMSMs can be expressed as follows:

$$t_e = 1.5P_n i_q\left[\left(L_d - L_q\right)i_d + \psi_f\right], \tag{2}$$

where $t_e$ and $P_n$ are, respectively, the electromagnetic torque and pole-pairs number of the motor.

Moreover, the motion equation of PMSMs can be expressed as follows:

$$J\frac{d\omega_m}{dt} = t_e - t_l - B\omega_m, \tag{3}$$

where $J$ and $\omega_m$ indicate, respectively, the rotational inertia and mechanical angular velocity of the motor; $t_l$ and $B$ represent the motor's load torque and friction coefficient, respectively.

*2.2. Vector Control of PMSMs.* The vector control of AC motors can solve the problem of efficient torque control of AC motors [30]. By regulating the excitation current $i_d$ and torque current $i_q$ in $d$-$q$ axes, the decoupling control of flux and torque can be realized for AC motors.

Till now, several vector control schemes have been developed for PMSMs in terms of different control methods on the excitation and torque currents [31, 32], e.g., the excitation current $i_d^* = 0$ scheme, the power factor $\cos\phi = 1$ scheme, the constant flux scheme, and the scheme of the maximum ratio of torque and current, to name a few. In this paper, the $i_d^* = 0$ scheme is applied for the vector control of PMSMs since it is easier to achieve the efficient current control of the motor [33].

Figure 1 describes a PMSM vector control system, where $\omega_m^*$, $i_q^*$, and $i_d^*$ are, respectively, the desired setpoint values for the speed and current controllers; the Clark and Park transforms are used for converting between the *abc*-*αβ* and *αβ*-*dq* coordinate systems, respectively; and the automatic speed regulator (ASR) and the automatic current regulator (ACR) are utilized for the speed and current controllers of the PMSM, which will be designed in the following sections of this paper. For more details on the vector control of PMSMs, the interested reader can refer to [34, 35] and the references therein.

## 3. Design of ASR Based on Modified LADRC

*3.1. Speed Controller Design Based on LADRC.* The LADRC consists of the linear tracking differentiator (LTD), linear extended state observer (LESO), and linear state error feedback (LSEF) [36]. Figure 2 depicts the structure of a LADRC system, where the role of LTD is to track the desired setpoint signal for an arranging transition process, thereby reducing the overshoot during the regulation of the system; the LESO is used to observe the extended states used for the state feedback and disturbance compensation of the system, and the LSEF has the effect of generating a control output to compensate for the total disturbance of the system [21]. The LADRC for the speed control of PMSMs in this paper is designed as follows.

*3.1.1. LTD.* The LTD utilized in this paper can be expressed as follows:

$$\begin{cases} e_0 = \omega_0 - \omega_m^*, \\ \dot{\omega}_0 = -re_0, \end{cases} \tag{4}$$

where $\omega_m^*$ is the input of LTD that denotes the desired setpoint of the mechanical angular velocity of the PMSM; $\omega_0$ is the output of LTD that denotes the desired mechanical angular velocity of the speed control; $e_0$ denotes the error between $\omega_m^*$ and $\omega_0$; and $r$ is the speed factor that affects the tracking speed of LTD.

*3.1.2. LESO.* From equations (2) and (3), the speed differential equation of PMSMs can be expressed as follows:

$$\frac{d\omega_m}{dt} = \frac{1.5}{J}P_n i_q\left[\left(L_d - L_q\right)i_d + \psi_f\right] - \frac{1}{J}\left(t_l + B\omega_m\right), \tag{5}$$

which can be simplified as follows:

$$\frac{d\omega_m}{dt} = \frac{1.5}{J}P_n\psi_f i_q + f, \tag{6}$$

where $f$ is called the total disturbance of the speed loop that can be expressed as follows:

$$f = \frac{1.5}{J}P_n i_q i_d\left(L_d - L_q\right) - \frac{1}{J}\left(t_l + B\omega_m\right) + \delta, \tag{7}$$

where $\delta$ stands for the total uncertain dynamics owing to the model inaccuracy and load disturbance of the system. Let $b_0 = 1.5P_n\psi_f/J$, $y = x_1 = \omega_m$, $x_2 = f$, and $u = i_q$, then equation (14) can be formulated as follows:

$$\dot{x}_1 = x_2 + b_0 u, \tag{8}$$

and the state-space equation of the system can be expressed as follows:

$$\begin{cases} \dot{x} = Ax + Bu + E\dot{f}, \\ y = Cx, \end{cases} \tag{9}$$

where $x = [x_1, x_2]^T$, $A = \begin{bmatrix} 0 & 1 \\ 0 & 0 \end{bmatrix}$, $B = [b_0, 0]^T$, $E = [0, 1]^T$, and $C = [1, 0]$. Then, according to the design method proposed in [21], the LESO for the extended state observation of the PMSM servo system can be designed as follows:

$$\begin{aligned} \dot{z} &= [A - LC]z + \begin{bmatrix} B & L \end{bmatrix}\begin{bmatrix} u \\ y \end{bmatrix} \\ &= \begin{bmatrix} -\beta_1 & 1 \\ -\beta_2 & 0 \end{bmatrix}\begin{bmatrix} z_1 \\ z_2 \end{bmatrix} + \begin{bmatrix} b_0 & \beta_1 \\ 0 & \beta_2 \end{bmatrix}\begin{bmatrix} u \\ y \end{bmatrix}, \end{aligned} \tag{10}$$

where $z = [z_1, z_2]^T$ is the extended state vector of the observer, i.e., the estimation of $x = [x_1, x_2]^T$; $L = [\beta_1, \beta_2]^T$ is the gain of the observer, which can be designed by placing

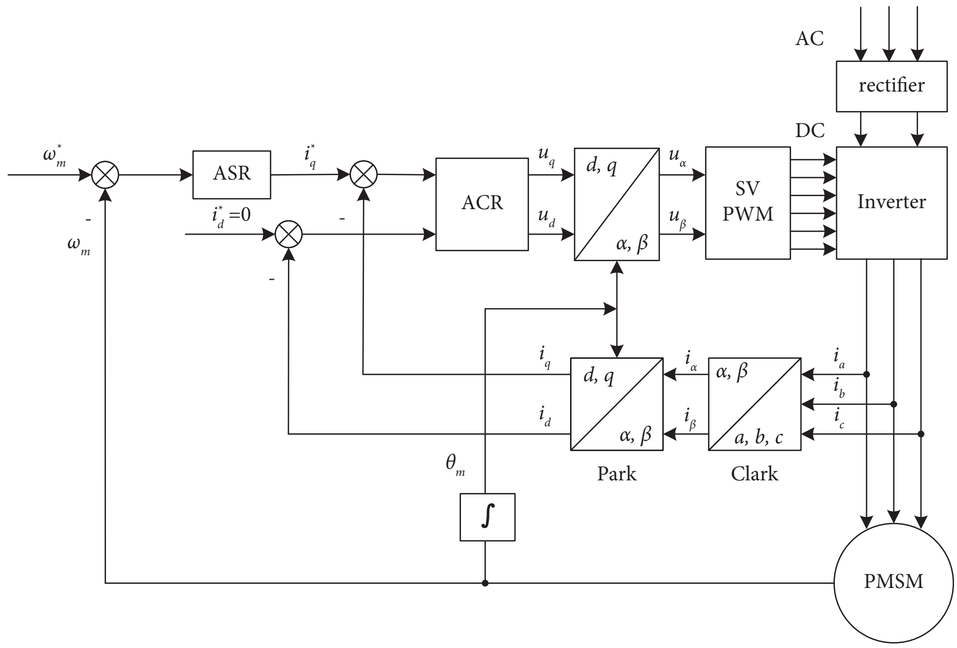


Figure 1: PMSM vector control system.

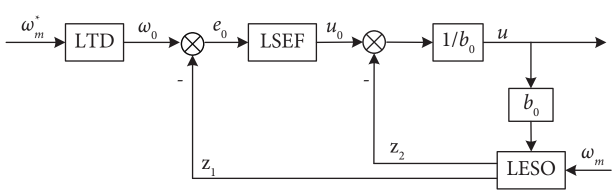


Figure 2: Structure of the LADRC system.

the poles of the characteristic equation to the stable pole $-\alpha$, i.e., the eigenvalue $\lambda$ should satisfy the following equation:

$$\begin{aligned} |\lambda I-(A-LC)| &= \begin{vmatrix} \lambda+\beta_1 & -1 \\ \beta_2 & \lambda \end{vmatrix} \\ &= \lambda^2+\beta_1\lambda+\beta_2 \\ &= (\lambda+\alpha)^2, \end{aligned} \tag{11}$$

where $I$ denotes the identity matrix. As such, the gain of the observer can be calculated as follows:

$$L=[\beta_1,\beta_2]^T=\left[2\alpha,\alpha^2\right]^T, \tag{12}$$

where $\alpha>0$ can be considered as the bandwidth of the LESO system. By appropriately selecting the bandwidth, the LESO can obtain an accurate estimation of the system's extended states, thereby achieving better control performance by compensating for disturbances.

*Remark 1.* The design of the bandwidth $\alpha$ is a tradeoff between the performance of tracking disturbances and the tolerance of sampling noises. Generally, on one hand, a large bandwidth can ensure the fast dynamics of the LESO in tracking the total disturbance. On the other hand, the heightened sensitivity to sampling noises will be an inevitable consequence of the large bandwidth.

*3.1.3. LSEF.* In this paper, the proportional control is used for the LSEF, which can be expressed as follows:

$$u_0=K_p\left(\omega_0-z_1\right), \tag{13}$$

where $K_p$ is the gain of the proportional controller; $\omega_0$ is the output of LTD, i.e., the desired mechanical angular velocity of the speed control loop; and $z_1$ is the estimation of the mechanical angular velocity $\omega_m$.

As depicted in Figure 2, to compensate for the total disturbance of the speed control loop, the control output $u$, which is also the desired $q$-axis current $i_q^*$ of the current control loop, can be expressed as follows:

$$u=\frac{u_0-z_2}{b_0}, \tag{14}$$

where $z_2$ is the estimation of the total disturbance.

*3.2. Modified LADRC Based on an Improved LESO.* The LESO expression in equation (10) can be rewritten as follows:

$$\begin{cases} e_1=z_1-x_1, \\ \dot{z}_1=z_2-\beta_1e_1+b_0u, \\ \dot{z}_2=-\beta_2e_1. \end{cases} \tag{15}$$

In the LADRC-based PMSM control system, the objective of LESO is to achieve convergence of observer outputs to the extended states, i.e., $z_1\longrightarrow x_1$ and $z_2\longrightarrow x_2$. From the abovementioned equations, it can be found that the dynamics of the observer are directly influenced by the observation error $e_1=z_1-x_1$. When the error is approaching zero, it is necessary to choose larger observer gains for accurate estimation of the total disturbance [37]. However, this choice would unfortunately come at the expense of deteriorating the observer's dynamic performance.

To overcome the aforementioned limitations, a new error formulation has been presented in [38] to improve the traditional LESO. Based on the new error concept, an improved LESO has been designed in this paper for observing internal and external disturbances of the PMSM control system.

From equation (15), we can derive that

$$\begin{cases} z_1 = e_1 + x_1, \\ z_2 = \dot{z}_1 + \beta_1 e_1 - b_0 u. \end{cases} \quad (16)$$

By combining equations (8) and (16), we can conclude that

$$\begin{cases} z_1 = e_1 + x_1, \\ z_2 = x_2 + \dot{e}_1 + \beta_1 e_1. \end{cases} \quad (17)$$

Hence, the error between $z_2$ and $x_2$ is $\dot{e}_1 + \beta_1 e_1$, which can be introduced into LESO, thereby obtaining the ILESO as follows:

$$\begin{cases} e_1 = z_1 - x_1, \\ \dot{z}_1 = z_2 - \beta_1 e_1 + b_0 u, \\ \dot{z}_2 = -\beta_2 (\dot{e}_1 + \beta_1 e_1), \end{cases} \quad (18)$$

and we can get the matrix equation of the ILESO as follows:

$$\begin{bmatrix} \dot{z}_1 \\ \dot{z}_2 \end{bmatrix} = \begin{bmatrix} -\beta_1 & 1 \\ 0 & -\beta_2 \end{bmatrix} \begin{bmatrix} z_1 \\ z_2 \end{bmatrix} + \begin{bmatrix} b_0 & \beta_1 & 0 \\ -b_0\beta_2 & 0 & \beta_2 \end{bmatrix} \begin{bmatrix} u \\ y \\ \dot{y} \end{bmatrix}. \quad (19)$$

Based on the theory of linear systems, the poles of the system can be placed at point $-\alpha$, i.e., the eigenvalue $\lambda$ should satisfy the following equation:

$$\begin{vmatrix} \lambda + \beta_1 & -1, \\ 0 & \lambda + \beta_2 \end{vmatrix} = \lambda^2 + (\beta_1 + \beta_2)\lambda + \beta_1\beta_2 = (\lambda + \alpha)^2. \quad (20)$$

As such, the gain vector of the observer can be calculated as follows:

$$L = [\beta_1, \beta_2]^T = [\alpha, \alpha]^T. \quad (21)$$

Finally, based on the abovementioned ILESO, the modified LADRC for the ASR of the PMSM control system can be expressed as follows:

$$\begin{cases} e_0 = \omega_0 - \omega_m^*, \\ \dot{\omega}_0 = -r e_0, \\ \dot{z}_1 = z_2 + b_0 u - \beta_1 (z_1 - y), \\ \dot{z}_2 = -\beta_2 [\dot{z}_1 - \dot{y} + \beta_1 (z_1 - y)], \\ u_0 = K_p (\omega_0 - z_1), \\ u = \dfrac{u_0 - z_2}{b_0}, \end{cases} \quad (22)$$

where $r$, $\alpha (\alpha = \beta_1 = \beta_2)$, and $K_p$ are the three parameters that should be tuned based on the control performance criteria of PMSMs.

*3.3. Error Analysis of the Improved LESO.* In this section, the error of the ILESO has been investigated based on the transfer function method. In terms of the theory of linear systems and the matrix equation of the ILESO in equation (19), the transfer function of $z = [z_1, z_2]^T$ can be calculated as follows:

$$z(s) = (sI - \overline{A})^{-1} \overline{B} u_l(s), \quad (23)$$

where $\overline{A} = \begin{bmatrix} -\beta_1 & 1 \\ 0 & -\beta_2 \end{bmatrix}$, $\overline{B} = \begin{bmatrix} b_0 & \beta_1 & 0 \\ -b_0\beta_2 & 0 & \beta_2 \end{bmatrix}$, $\beta_1 = \beta_2 = \alpha$, $u_l(s) = [u(s), y(s), \dot{y}(s)]^T$, $\dot{y}(s) = sy(s)$, and $s$ is the Laplace operator.

In accordance with equation (23), the transfer functions of $z_1$ and $z_2$ can be calculated as follows:

$$\begin{cases} z_1(s) = \dfrac{b_0 s}{(s+\alpha)^2} u(s) + \dfrac{2\alpha s + \alpha^2}{(s+\alpha)^2} y(s), \\ z_2(s) = \dfrac{-b_0\alpha}{s+\alpha} u(s) + \dfrac{\alpha s}{s+\alpha} y(s). \end{cases} \quad (24)$$

Let $e_1 = z_1 - y$ and $e_2 = z_2 - f$, then we can obtain the transfer functions of $e_1$ and $e_2$ as follows:

$$\begin{cases} e_1(s) = z_1(s) - y(s) \\ = \dfrac{b_0 s}{(s+\alpha)^2} u(s) + \dfrac{-s^2}{(s+\alpha)^2} y(s) \\ e_2(s) = z_2(s) - f(s) \\ = z_2(s) - sy(s) + b_0 u(s) \\ = \dfrac{b_0 s}{s+\alpha} u(s) + \dfrac{-s^2}{s+\alpha} y(s), \end{cases} \quad (25)$$

where $f(s) = \dot{y}(s) - b_0 u(s) = sy(s) - b_0 u(s)$ can be obtained from equation (8).

Considering equation (14) and without loss of generality, we assume that $u$ is a step signal and $y$ is a ramp signal. Their transfer functions are, respectively, $u(s) = K_u/s$ and $y(s) = K_y/s^2$, where $K_u$ and $K_y$ are signal amplitudes. Then, by utilizing the final value theorem, the steady-state error of the ILESO can be calculated as follows:

$$\begin{cases} e_{ss1} = \lim_{s\longrightarrow 0} se_1(s) \\ = \lim_{s\longrightarrow 0} s\left[\dfrac{b_0 s}{(s+\alpha)^2}u(s) + \dfrac{-s^2}{(s+\alpha)^2}y(s)\right] \\ = \lim_{s\longrightarrow 0} s\left[\dfrac{b_0 s}{(s+\alpha)^2}\dfrac{K_u}{s} + \dfrac{-s^2}{(s+\alpha)^2}\dfrac{K_y}{s^2}\right] = 0, \\ e_{ss2} = \lim_{s\longrightarrow 0} se_2(s) \\ = \lim_{s\longrightarrow 0} s\left[\dfrac{b_0 s}{s+\alpha}u(s) + \dfrac{-s^2}{s+\alpha}y(s)\right] \\ = \lim_{s\longrightarrow 0} s\left[\dfrac{b_0 s}{s+\alpha}\dfrac{K_u}{s} + \dfrac{-s^2}{s+\alpha}\dfrac{K_y}{s^2}\right] = 0. \end{cases} \tag{26}$$

*Remark 2.* It is worth noting that the $u_0$ in $u$ is the output of a proportional controller, which means it is reasonable to take $u$ as a step signal whether the desired speed of PMSM is a step signal or a ramp signal. It is also a logical idea to take $y$ as a ramp signal because the state estimation in the acceleration or deceleration of PMSM is the biggest challenge for the state observer.

## 4. Design of ACR Based on PI Controllers

From the voltage equations in equation (1), it can be observed that the stator current will generate the coupled electromotive forces in $d$-$q$ axes. Through a simple formula manipulation, the decoupled voltage equations can be expressed as follows:

$$\begin{cases} u_{d0} = u_d + \omega_e L_q i_q = Ri_d + L_d \dfrac{di_d}{dt}, \\ u_{q0} = u_q - \omega_e\left(L_d i_d + \psi_f\right) = Ri_q + L_q \dfrac{di_q}{dt}, \end{cases} \tag{27}$$

where $u_{d0}$ and $u_{q0}$ are the voltages in $d$-$q$ axes after current decoupling. Based on the abovementioned voltage equations, the transfer function of stator currents can be obtained via the Laplace transform as follows:

$$I(s) = G(s)U(s), \tag{28}$$

where $I(s) = [I_d(s), I_q(s)]^T$ is the transfer functions of $i_d$ and $i_q$; $U(s) = [U_{d0}(s), U_{q0}(s)]^T$ is the transfer functions of $u_{d0}$ and $u_{q0}$; and $G(s) = \begin{bmatrix} R + sL_d & 0 \\ 0 & R + sL_q \end{bmatrix}^{-1}$ is the model of the ACR's control object. In this paper, PI controllers are chosen for the control of $U(s)$, which can be expressed as follows:

$$\begin{cases} U_{d0}(s) = \left(K_{pd} + \dfrac{K_{id}}{s}\right)\left(I_d^*(s) - I_d(s)\right), \\ U_{q0}(s) = \left(K_{pq} + \dfrac{K_{iq}}{s}\right)\left(I_q^*(s) - I_q(s)\right), \end{cases} \tag{29}$$

where $I_d^*(s)$ and $I_q^*(s)$ are, respectively, the reference values of $I_d(s)$ and $I_q(s)$; $K_{pd}$ and $K_{pq}$ are the proportional gains of the PI controllers; and $K_{id}$ and $K_{iq}$ are the corresponding integral gains of the controllers.

In this paper, the initial gains of PI controllers are designed based on the internal model control scheme [8]. Figure 3 describes a block diagram of the internal model control (IMC) system, where $G(s)$ is the control object; $\widehat{G}(s)$ is the internal model of $G(s)$; and $C(s)$ is the internal model controller. Through an equivalent transformation, an equivalent block diagram can be acquired as shown in Figure 4, where $F(s)$ is the equivalent internal model controller that can be calculated as follows:

$$F(s) = [I - C(s)\widehat{G}(s)]^{-1}C(s). \tag{30}$$

According to the theory of IMC [39], we can design the internal model controller as follows:

$$C(s) = \widehat{G}^{-1}(s)L(s), \tag{31}$$

where $L(s) = r/(s + r)$ and $\gamma$ is the bandwidth of the current loop. Based on equation (31) and the model of the current loop in equation (28), the equivalent internal model controller in equation (30) can be calculated as follows:

$$F(s) = \gamma\begin{bmatrix} L_d + \dfrac{R}{s} & 0 \\ 0 & L_q + \dfrac{R}{s} \end{bmatrix}. \tag{32}$$

As such, by comparing equations (29) and (32), the gains of the PI controllers can be determined as follows:

$$\begin{cases} K_{pd} = \gamma L_d, \\ K_{id} = \gamma R, \\ K_{pq} = \gamma L_q, \\ K_{iq} = \gamma R, \end{cases} \tag{33}$$

where $\gamma = 2\pi/\tau$ and $\tau$ is the time constant of the motor that can be set as follows:

$$\tau = \min\left\{\frac{L_d}{R}, \frac{L_q}{R}\right\}. \tag{34}$$

Finally, by combining the feedforward decoupling scheme, the ACR of the PMSM vector control system can be designed as follows:

$$\begin{cases} u_d = u_{d0} - \omega_e L_q i_q, \\ u_q = u_{q0} + \omega_e\left(L_d i_d + \psi_f\right). \end{cases} \tag{35}$$

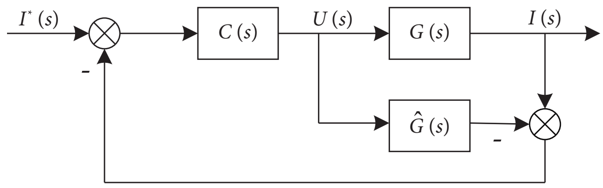


Figure 3: Block diagram of the IMC system.

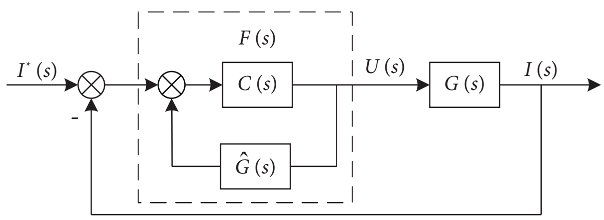


Figure 4: Equivalent block diagram of the IMC system.

*Remark 3.* It should be pointed out that due to the inevitable modeling errors of the PMSM control system, the parameters of the PI controllers designed based on the internal model control scheme can only serve as initial values and require further optimization. These initial values provide a magnitude range for the parameters to be tuned, which offers a reasonable search space for further parameter optimization.

## 5. Tuning of Controller Parameters Based on the PSO-AWDV Algorithm

In the abovementioned control system, several controller parameters need to be adjusted to achieve optimal control performance. Typically, controller parameter tuning is a time-consuming and labor-intensive task. Especially, it is a challenge to obtain the optimal solution due to the coupling effect of the dual-loop control system of PMSMs. Therefore, in this paper, we utilize an improved PSO variant, PSO with adaptive weighted delay velocity (PSO-AWDV), developed in our previous work to tune the speed and current controllers of the PMSM control system simultaneously.

*5.1. PSO-AWDV Algorithm.* The PSO algorithm, developed by Kennedy and Eberhart, is an intelligent optimization algorithm simulating the behavior of biological populations, such as bird flocks and fish schools [40, 41]. Since the original PSO algorithm was proposed, numerous variants have been developed to address its deficiencies, such as local trapping and premature convergence. The schemes of the variants include introducing different strategies, modifying parameter settings, and combining them with other algorithms, which are utilized to enhance the performance and convergence speed of the PSO algorithm [42, 43].

In the PSO-AWDV algorithm [44], the velocity and position vectors of the particles are updated as follows:

$$\begin{cases} \overrightarrow{V}_i^{k+1} = w\overrightarrow{V}_i^{k} + (1-w)\overrightarrow{V}_i^{k-1} \\ +c_1r_1\left(\overrightarrow{P}_i^{k} - \overrightarrow{X}_i^{k}\right) + c_2r_2\left(\overrightarrow{G}^{k} - \overrightarrow{X}_i^{k}\right), \\ \overrightarrow{X}_i^{k+1} = \overrightarrow{X}_i^{k} + \overrightarrow{V}_i^{k+1}, \end{cases} \tag{36}$$

where $\overrightarrow{V}_i^{k}$ and $\overrightarrow{X}_i^{k}$ are, respectively, the $i$-th particle's velocity and position vectors at the $k$-th iteration; $\overrightarrow{P}_i^{k}$ and $\overrightarrow{G}^{k}$ indicate the personal best position of the $i$-th particle and the global best position of the swarm up to the $k$-th iteration, respectively; $w$ is the inertia weight of the velocity vector $\overrightarrow{V}_i^{k}$; and $1-w$ is the inertia weight for the delayed velocity vector $\overrightarrow{V}_i^{k-1}$ with $0 < w < 1$.

The inertia weight $w$ can be regulated adaptively according to the evolutionary state of the swarm as follows:

$$w = 1 - \frac{a}{1+\exp\left(b\cdot E^k\right)}, \tag{37}$$

where $a$ and $b$ are the two parameters for adjusting the convergence performance of the PSO-AWDV algorithm, and $E^k$ is the estimation of the evolutionary state of the swarm at the $k$-th iteration, which is defined as follows:

$$E^k = \frac{f_{\max}^k - f_{\min}^k}{f_{\max}^k}, \tag{38}$$

where $f_{\max}^k$ and $f_{\min}^k$ are the maximal and minimal fitness values of the particles at the $k$-th iteration, respectively. Besides, $c_1$ and $c_2$ in equation (36) are the acceleration factors that can be calculated by

$$\begin{cases} c_1 = \left(c_{1i} - c_{1f}\right) \times \dfrac{k_{\mathrm{m}} - k}{k_{\mathrm{m}}} + c_{1f}, \\ c_2 = \left(c_{2i} - c_{2f}\right) \times \dfrac{k_{\mathrm{m}} - k}{k_{\mathrm{m}}} + c_{2f}, \end{cases} \tag{39}$$

where $c_{1i}\,(c_{2i})$ and $c_{1f}\,(c_{2f})$ indicate the initial and final values of the acceleration factors, respectively, and $k_{\mathrm{m}}$ is the maximal iteration number for the optimization. $r_1$ and $r_2$ are uniformly distributed random numbers between [0, 1] in the PSO-AWDV algorithm. The interested reader can refer to [44, 45] for more details on the effectiveness and superiority of the PSO-AWDV algorithm as well as its stability analysis.

*5.2. Controller Parameter Tuning.* Based on the abovementioned discussions, the controller parameter tuning in this paper can be transformed into a parameter optimization problem to minimize the following performance criteria:

$$J(\mathbf{K}^*) = \arg\min_{\mathbf{K}} J(\mathbf{K}), \tag{40}$$

where $\mathbf{K} = [r, \alpha, K_p, K_{pd}, K_{id}, K_{pq}, K_{iq}]^T$ is the vector composed of controller parameters to be tuned; $\mathbf{K}^*$ represents the optimal values of the controller parameter vector; and $J(\cdot)$ is the integral of time-weighted absolute error (ITAE) optimization criterion, which can be expressed as follows:

$$J(\mathbf{K}) = \int_0^{T_f} t|e(t)|dt, \tag{41}$$

where $T_f$ is the terminal time for calculating the optimization criteria and $e(t)$ represents the control deviation of the system influenced by the controller parameters.

Figure 5 describes the flowchart for the aforementioned controller parameter optimization. The optimization process begins with the initialization of the particle swarm using controller parameter vectors. Subsequently, the control system's parameters are configured to evaluate the optimization criteria following its operation. Once all particles complete their respective routines, the particle swarm will be updated according to the PSO-AWDV algorithm. The optimal control parameters will ultimately be generated as the output if the predefined stop criteria are met. Otherwise, the abovementioned procedure will be iteratively repeated till the end.

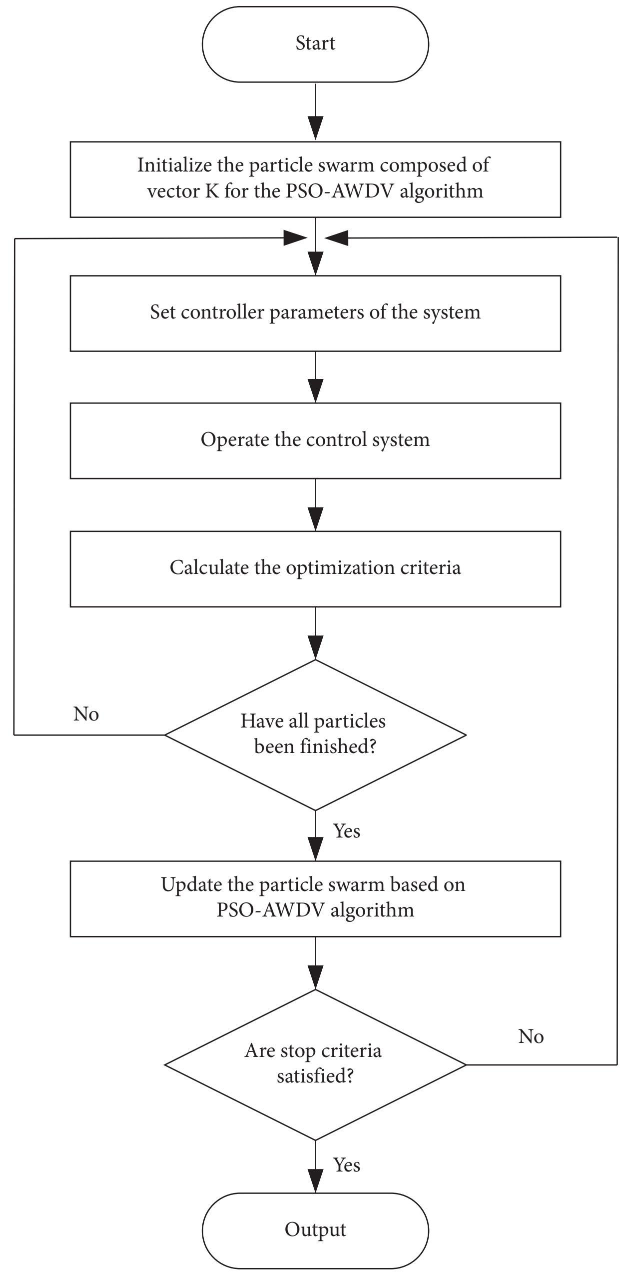


Figure 5: Flowchart of controller parameter optimization.

## 6. Performance Evaluations

To validate the performance of the designed control system, we will conduct performance comparisons for different speed-loop controllers including the PI controller, the LADRC controller, and the MLADRC controller, through both simulation and experiment, while maintaining the current loop controller as a PI controller.

The PMSM parameters for simulation and experiment are given as follows: pole-pairs number $P_n = 4$; rotational inertia $J = 0.0000189\ \text{kg}\cdot m^2$; stator resistance $R_s = 0.33\ \Omega$; $d$-axis stator inductance $L_d = 0.9$ mH; $q$-axis stator inductance $L_q = 0.9$ mH; and rotor magnet flux linkage $\psi_f = 0.012$ Wb.

*6.1. Simulation Results.* We use the MATLAB/Simulink platform for the simulation study of the PMSM control system. In the simulation, we start the motor under no-load conditions with a given speed of 1000 rpm. Then, we add a 0.4 Nm load to the PMSM at the moment of 0.2 seconds after the speed is stabilized. The parameters of the current-loop PI controller are set as 20 and 768 for the proportional and integral gains, respectively. For the speed-loop PI controller, the proportional and integral gains are set as 0.07 and 0.5, respectively. For LADRC and MLADRC controllers, the parameters are set as $\alpha = 5000$, $r = 200$, and $K_p = 250$.

Figure 6 shows the motor speed response curves in the simulation, while Figure 7 illustrates the corresponding motor electromagnetic torque variation curves. In the figures, the results for the three controllers are represented by blue, black, and red dotted lines, respectively. Table 1 provides the specific numerical values for speed overshoot during the startup (denoted as overshoot), speed fluctuation when the load changes (denoted as fluctuation), both of them are expressed in percentage, and the time for the speed to recover after fluctuations (denoted as recovery time).

It is evident that compared to the PI controller, the LADRC and MLADRC approaches exhibit faster response and zero overshoot during the motor startup thanks to the arranging transition process of LTD. In comparison to the other two controllers, the MLADRC presented in this study demonstrates a smaller overshoot and shorter recovery time in the case of load disturbances.

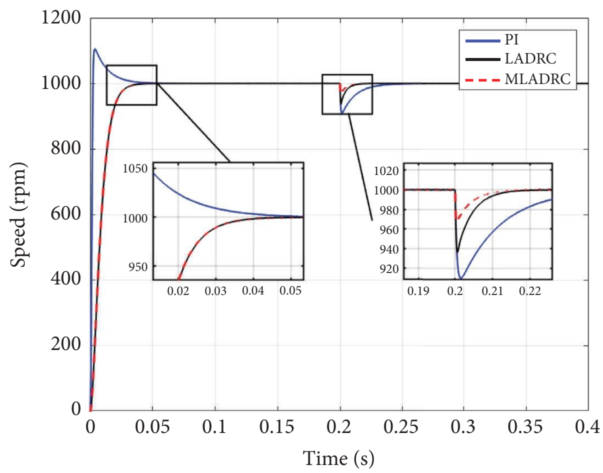


FIGURE 6: Speed response for step signal in simulation.

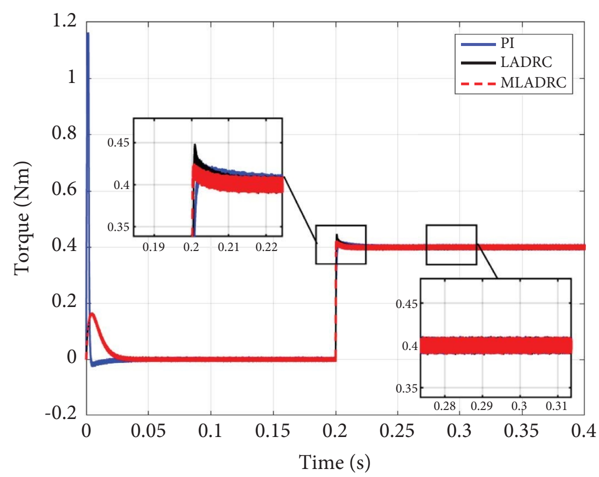


FIGURE 7: Electromagnetic torque response for step signal in simulation.

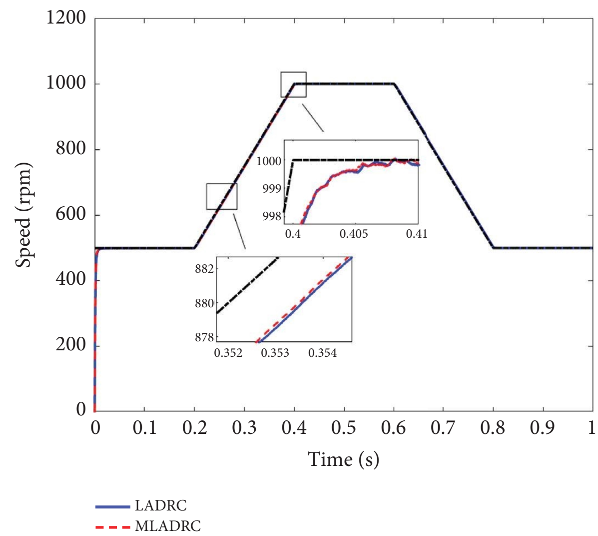


FIGURE 8: Speed response for ramp signal in simulation.

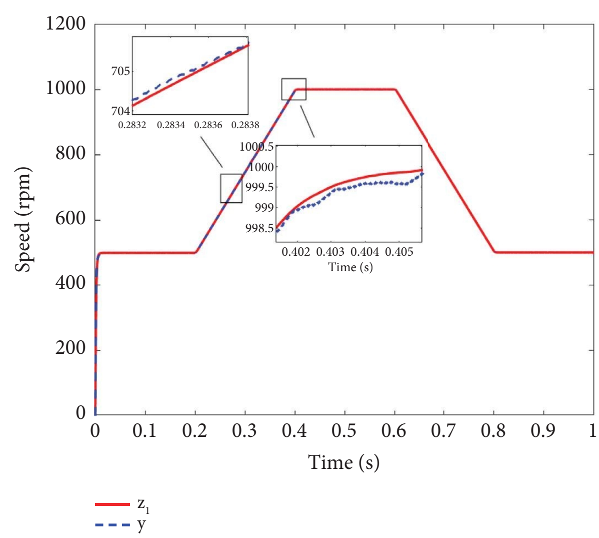


FIGURE 9: Speed estimation by LESO in simulation.

TABLE 1: Performance comparison in simulation.

| Controllers | Overshot | Fluctuation (%) | Recovery time (s) |
|---|---|---|---|
| PI | 10.4% | 8.80 | 0.100 |
| LADRC | — | 4.01 | 0.068 |
| MLADRC | — | 3.97 | 0.062 |

In the abovementioned simulation, the given reference speed is a constant value, i.e., a step signal. To further compare the performance of MLADRC and LADRC, we also study the case of the control system tracking a ramp signal. As shown in Figure 8, both controllers can achieve a relatively small speed control error. Comparatively, MLADRC exhibits better tracking performance due to the more accurate estimation results of ILESO for system states and disturbances. Figures 9 and 10 depict, respectively, the results of speed estimation by LESO and ILESO, where $y$ is the measurement of speed, and $z_1$ is the speed estimation. Clearly, the estimation results of ILESO are closer to the actual measured values.

As such, we can conclude that the MLADRC proposed in this study exhibits better performance for load disturbance resistance. This is mainly attributed to the enhanced accuracy of disturbance observation through the ILESO, allowing the control system to promptly compensate for disturbances and achieve a smoother control response.

*6.2. Experiment Results.* To further validate the performance of the MLADRC controller, motor control experiments are conducted using the multimotor drive control experimental platform as shown in Figure 11. The experimental platform has a PMSM with a rated speed of 3000 rpm, a rated torque of 0.637 Nm, a rated voltage of 36 V, a rated output power of 200 W, and a switching frequency of 15 kHz. The power supply for the platform is AC 220 V, which is rectified to provide a DC input for the inverter. The PMSM is connected to a DC motor through a coupling to create a load platform.

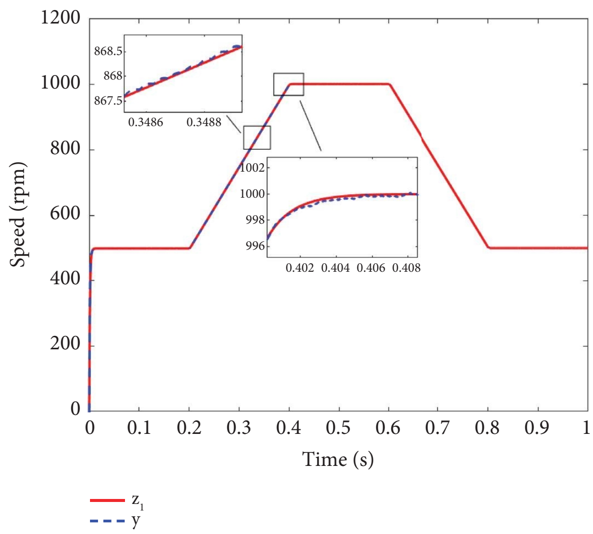


Figure 10: Speed estimation by ILESO in simulation.

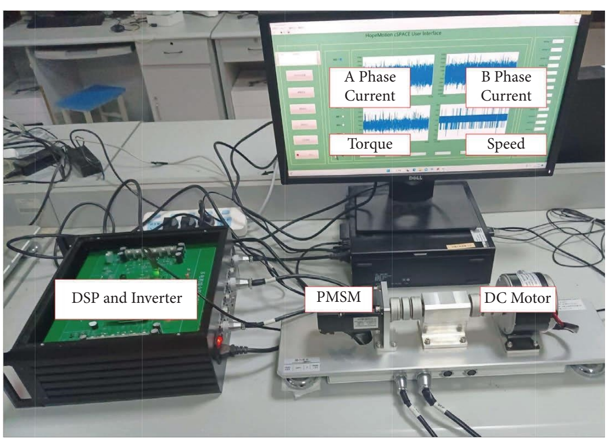


Figure 11: Multimotor drive control experimental platform.

After designing the motor control algorithm in the MATLAB/Simulink platform, it is downloaded to the DSP controller on the lower-level device via a JTAG interface. Information such as current, speed, and torque is collected and sent back to the upper-level computer for display and analysis.

During the experiment, identical PI controllers are employed for current loop control to ensure a fair comparison of the performance among different speed-loop controllers in a practical PMSM control system. The parameters of the current-loop PI controller are set as 0.2 and 0.02 for the proportional and integral gains, respectively. For the speed-loop PI controller, the proportional and integral gains are set as 0.04 and 0.00008, respectively. For LADRC and MLADRC controllers, the parameters are set as $\alpha = 100$ and $K_p = 6$.

For each experiment, it has a total runtime of 30 seconds with a sampling interval of 0.001 seconds. We first start the motor under no-load conditions with a given speed of 1000 rpm. To compare the startup performance of the controllers, it should be mentioned that the LTD module is

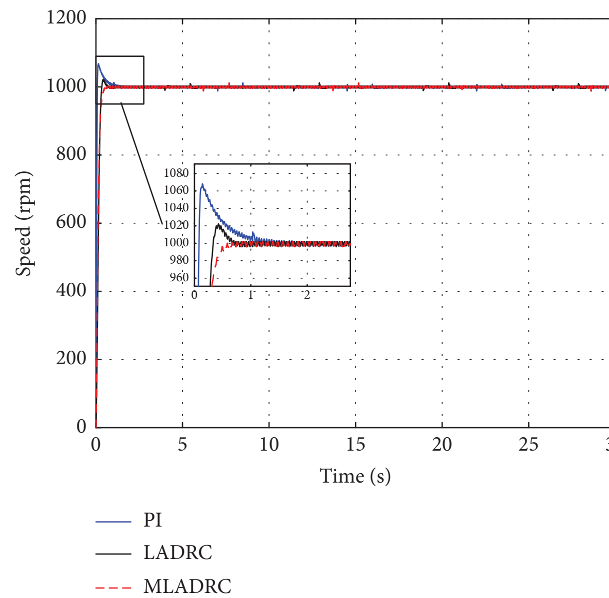


Figure 12: Speed response for the startup.

Table 2: Performance comparison for the startup.

| Controllers | Overshoot | Settling time (s) |
|---|---|---|
| PI | 6.8% | 1.30 |
| LADRC | 2.2% | 0.70 |
| MLADRC | — | 0.58 |

not incorporated into the LADRC and MLADRC controllers. Figure 12 manifests the motor speed response curves in the experiment. Table 2 presents the speed overshoot and settling time during the startup. It can be observed that the MLADRC controller can achieve zero overshoot and a shorter settling time when compared to both PI and LADRC controllers. Therefore, the experiment result indicates that the MLADRC controller exhibits superior performance during the motor startup process.

Furthermore, under the same conditions with a given speed of 1000 rpm, the motor is started under no-load conditions. The parameters of the current-loop PI controller are set as 0.2 and 0.02 for the proportional and integral gains, respectively. After the speed is stabilized, a load fluctuation of $\pm 0.36$ Nm is applied to the motor at different time and the speed changes are recorded as shown in Figure 13. Table 3 displays three controllers' speed fluctuations and recovery times in response to load changes. The experimental results also confirm that the MLADRC controller is capable of recovering to the target speed in the shortest time with minimal fluctuation during load variations, further highlighting its disturbance-rejection capability.

To further validate the performance of the control algorithm in the acceleration and deceleration control of PMSM, we set the reference speed for the motor to 500 rpm and 1000 rpm at the initial moment and then reversed the reference speeds to 1000 rpm and 500 rpm at the moment of 7 seconds. Figures 14 and 15 illustrate the speed response

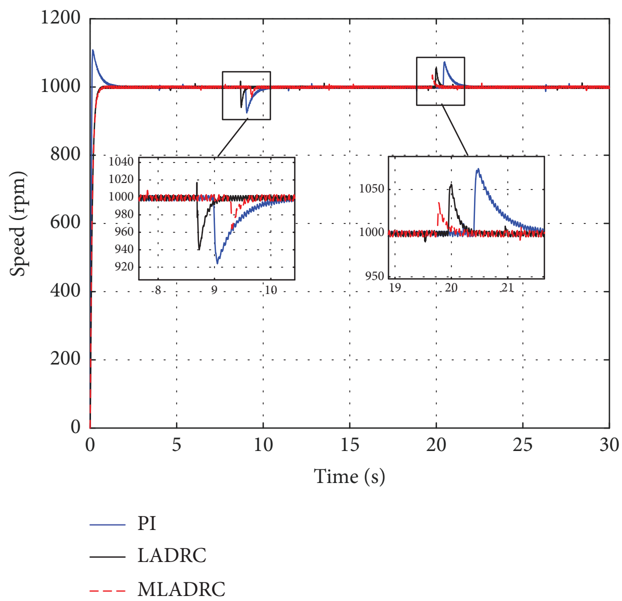


Figure 13: Speed response for load fluctuations.

Table 3: Performance comparison for load fluctuations.

| Controllers | Fluctuation (%) | Recovery time (s) |
|---|---|---|
| PI | 7.6 | 0.17 |
| LADRC | 5.8 | 0.10 |
| MLADRC | 4.1 | 0.05 |

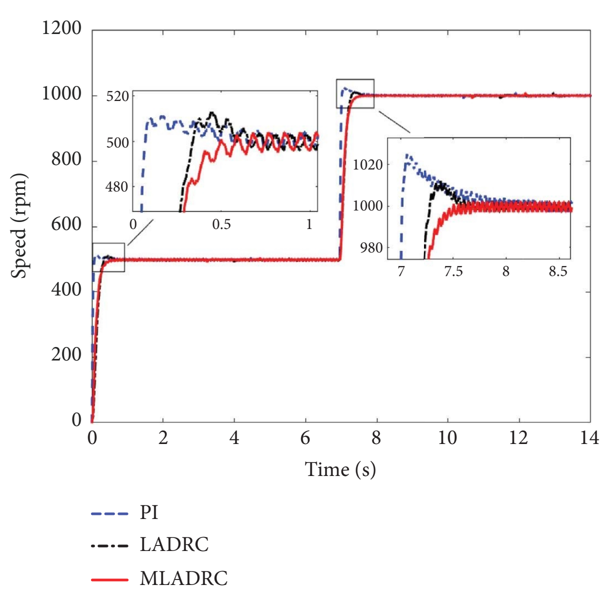


Figure 14: Speed response for acceleration.

curves for the three controllers. Tables 4 and 5 provide comparisons of the experimental results, which can reaffirm the superior performance of MLADRC compared to the other two controllers.

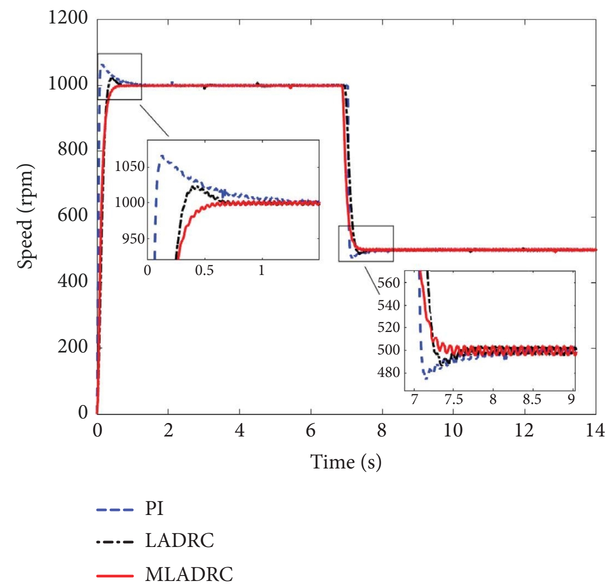


Figure 15: Speed response for deceleration.

Table 4: Performance comparison for acceleration.

| Controllers | Overshot | Recovery time (s) |
|---|---|---|
| PI | 2.4% | 1.247 |
| LADRC | 2.5% | 0.951 |
| MLADRC | — | 0.668 |

Table 5: Performance comparison for deceleration.

| Controllers | Overshot | Recovery time (s) |
|---|---|---|
| PI | 6.8% | 1.770 |
| LADRC | 2.2% | 1.465 |
| MLADRC | — | 0.731 |

## 7. Conclusion

In this paper, a PMSM dual-loop control system has been devised by integrating LADRC and PI controllers. First, an improved LESO with excellent observation capacities has been introduced to serve as the foundation for the development of a modified LADRC approach tailored for regulating the speed of PMSMs. Based on the improved LESO, a modified LADRC has been developed for the speed control of PMSMs. Furthermore, we harnessed the internal model control scheme to initialize the parameters of the PI-based current controllers. To fine-tune the entire PMSM control system, an improved PSO algorithm has been employed for optimizing the controller parameters, contributing to the system's overall performance. Finally, a series of simulations and experiments have been conducted to validate the effectiveness and superiority of our proposed approach, which outperforms both the traditional PI controller and the original LADRC controller.

Over the past few years, the networked control of multiple motors has emerged as a prominent area of research [46, 47]. Consequently, we aim to extend our previous accomplishments to enhance the control performance in the synchronized networked control of multiple motors based on some advanced control algorithms [48, 49].

## Data Availability

The data used to support the findings of this study are available on request from the corresponding author.

## Conflicts of Interest

The authors declare that they have no conflicts of interest.

## Acknowledgments

This research was supported by the Natural Science Foundation of Shandong Province of China (approved grant: ZR2023MF067) and the National Natural Science Foundation of China (approved grants: 62233012 and 62273211).

## References

[1] L. Qu, W. Qiao, and L. Qu, "An extended-state-observer-basedsliding-mode speed control for permanent-magnet synchronous motors," *IEEE Journal of Emerging and Selected Topics in Power Electronics*, vol. 9, no. 2, pp. 1605–1613, 2021.

[2] H. Liu, Y. Chen, H. Li, B. Zang, and H. Wang, "Active disturbance rejection position servo control of permanent magnet synchronous motor based on improved extended state observer," in *Proceedings of the 2021 24th International Conference on Electrical Machines and Systems*, pp. 1938–1942, Gyeongju, South Korea, October 2021.

[3] F. Wang and L. He, "FPGA-based predictive speed control for PMSM system using integral sliding-mode disturbance observer," *IEEE Transactions on Industrial Electronics*, vol. 68, no. 2, pp. 972–981, 2021.

[4] L. Qu, W. Qiao, and L. Qu, "Active-disturbance-rejection-basedsliding-mode current control for permanent-magnet synchronous motors," *IEEE Transactions on Power Electronics*, vol. 36, no. 1, pp. 751–760, 2021.

[5] X. Cai, Z. Zhang, J. Wang, and R. Kennel, "Optimal control solutions for PMSM drives: a comparison study with experimental assessments," *IEEE Journal of Emerging and Selected Topics in Power Electronics*, vol. 6, no. 1, pp. 352–362, 2018.

[6] X. Wang, B. Ufnalski, and L. M. Grzesiak, "Adaptive speed control in the PMSM drive for a non-stationary repetitive process using particle swarms," in *Proceedings of the 10th International Conference on Compatibility, Power Electronics and Power Engineering*, pp. 464–471, Bydgoszcz, Poland, June 2016.

[7] Y. Yan, J. Yang, Z. Sun, S. Li, and H. Yu, "Non-linear-disturbance-observer-enhanced MPC for motion control systems with multiple disturbances," *IET Control Theory and Applications*, vol. 14, no. 1, pp. 63–72, 2020.

[8] C. Liu, G. Luo, Z. Xue, Z. Zhou, and Z. Chen, "A PMSM speed servo system based on internal model control with extended state observer," in *Proceedings of the 43rd Annual Conference of the IEEE Industrial Electronics Society*, pp. 1729–1734, Beijing, China, October 2017.

[9] B. Zhang, Y. Pi, and Y. Luo, "Fractional order sliding-mode control based on parameters auto-tuning for velocity control of permanent magnet synchronous motor," *ISA Transactions*, vol. 51, no. 5, pp. 649–656, 2012.

[10] J. Ren, Y. Ye, G. Xu, Q. Zhao, and M. Zhu, "Uncertainty-and-disturbance-estimator-based current control scheme for PMSM drives with a simple parameter tuning algorithm," *IEEE Transactions on Power Electronics*, vol. 32, no. 7, pp. 5712–5722, 2017.

[11] Z. Hao, Y. Tian, Y. Yang, Y. Gong, Z. Hao, and J. Zhang, "Sensorless control based on the uncertainty and disturbance estimator for IPMSMs with periodic loads," *IEEE Transactions on Industrial Electronics*, vol. 70, no. 5, pp. 5085–5093, 2023.

[12] Y. Cao, J. Wang, and W. Shen, "High-performance PMSM self-tuning speed control system with a low-order adaptive instantaneous speed estimator using a low-cost incremental encoder," *Asian Journal of Control*, vol. 23, no. 4, pp. 1870–1884, 2021.

[13] J. Han, "From PID to active disturbance rejection control," *IEEE Transactions on Industrial Electronics*, vol. 56, no. 3, pp. 900–906, 2009.

[14] Y. Zuo, X. Ge, Y. Zheng, Y. Chen, H. Wang, and A. T. Woldegiorgis, "An adaptive active disturbance rejection control strategy for speed-sensorless induction motor drives," *IEEE Transactions on Transportation Electrification*, vol. 8, no. 3, pp. 3336–3348, 2022.

[15] B. Du, S. Wu, S. Han, and S. Cui, "Application of linear active disturbance rejection controller for sensorless control of internal permanent-magnet synchronous motor," *IEEE Transactions on Industrial Electronics*, vol. 63, no. 5, pp. 3019–3027, 2016.

[16] Z. Kuang, B. Du, S. Cui, and C. C. Chan, "Speed control of load torque feedforward compensation based on linear active disturbance rejection for five-phase PMSM," *IEEE Access*, vol. 7, pp. 159787–159796, 2019.

[17] Y. Liu, J. Wen, D. Xu, Z. Huang, and H. Zhou, "The decoupled vector-control of PMSM based on nonlinear multi-input multi-output decoupling ADRC," *Advances in Mechanical Engineering*, vol. 12, 12 pages, 2020.

[18] Z. Rong and Q. Huang, "A new PMSM speed modulation system with sliding mode based on active-disturbance-rejection control," *Journal of Central South University*, vol. 23, no. 6, pp. 1406–1415, 2016.

[19] C. Liu, G. Luo, W. Tu, and H. Wan, "Servo systems with closed-loops based on active disturbance rejection controllers," *Proceedings of CSEE*, vol. 37, no. 23, pp. 7032–7039, 2017.

[20] H. Pan, "Research on a new active disturbance rejection control algorithm," *Control Engineering China*, vol. 27, no. 4, pp. 728–732, 2020.

[21] Z. Gao, "Scaling and bandwidth-parameterization based controller tuning," in *Proceedings of American Control Conference*, pp. 4989–4996, Denver, CO, USA, June 2003.

[22] X. Feng, S. Xie, Z. Zhang, Y. Chen, H. Qin, and C. Zhao, "Research on speed loop control of IPMSM based on Fuzzy linear active disturbance rejection control," *Energy Reports*, vol. 8, pp. 804–812, 2022.

[23] Z. Zhang, Y. Chen, L. Tan, and C. Zhao, "Torque ripple suppression for permanent-magnet synchronous motor based on enhanced LADRC strategy," *Journal of Electrical Engineering and Technology*, vol. 17, no. 5, pp. 2753–2760, 2022.

[24] J. Song, W. Zheng, and Y. Niu, "Self-triggered sliding mode control for networked PMSM speed regulation system: a PSO-optimized super-twisting algorithm," *IEEE Transactions on Industrial Electronics*, vol. 69, no. 1, pp. 763–773, 2022.

[25] J. Song, Y. Wang, Y. Niu, H.-K. Lam, S. He, and H. Liu, "Periodic event-triggered terminal sliding mode speed control for networked PMSM system: a GA-optimized extended state observer approach," *IEEE*, vol. 27, no. 5, pp. 4153–4164, 2022.

[26] J. Yang, L. Yu, X. Yang, and J. Zhou, "PI controller parameter setting of PMSM speed control system based on pigeon-inspired optimization algorithm," in *Proceedings of the 6th IEEE Advanced Information Technology, Electronic and Automation Control Conference*, pp. 1996–2000, Beijing, China, October 2022.

[27] Z. Yin, L. Gong, C. Du, J. Liu, and Y. Zhong, "Integrated position and speed loops under sliding-mode control optimized by differential evolution algorithm for PMSM drives," *IEEE Transactions on Power Electronics*, vol. 34, no. 9, pp. 8994–9005, 2019.

[28] G. Wang, M. Valla, and J. Solsona, "Position sensorless permanent magnet synchronous machine drives–a review," *IEEE Transactions on Industrial Electronics*, vol. 67, no. 7, pp. 5830–5842, 2020.

[29] C. Wang, B. Liu, X. Fan, and P. Yang, "Rotor position angle control of permanent magnet synchronous motor based on sliding mode extended state observer," *Systems Science and Control Engineering*, vol. 10, no. 1, pp. 757–766, 2022.

[30] B. K. Bose, "The past, present, and future of power electronics," *IEEE Industrial Electronics Magazine*, vol. 3, no. 2, pp. 7–12, 2009.

[31] X. Tang, Z. Zhang, X. Liu, C. Liu, M. Jiang, and Y. Song, "A novel field-oriented control algorithm for permanent magnet synchronous motors in 60° coordinate systems," *Actuators*, vol. 12, no. 2, p. 92, 2023.

[32] V. M. Bida, D. V. Samokhvalov, and F. S. Al-Mahturi, "PMSM vector control techniques–a survey," in *Proceedings of IEEE Conference of Russian Young Researchers in Electrical and Electronic Engineering*, pp. 577–581, Saint Petersburg, Russia, September 2018.

[33] Y. Wang, S. Fang, and D. Huang, "An improved model-free active disturbance rejection deadbeat predictive current control method of PMSM based on data-driven," *IEEE Transactions on Power Electronics*, vol. 38, no. 8, pp. 9606–9616, 2023.

[34] J. Yang, W.-H. Chen, S. Li, L. Guo, and Y. Yan, "Disturbance/uncertainty estimation and attenuation techniques in PMSM drives–A survey," *IEEE Transactions on Industrial Electronics*, vol. 64, no. 4, pp. 3273–3285, 2017.

[35] P. Du, J. Liu, K. Lv, L. Pei, and L. Li, "A novel control system simulation modeling method considering the real hardware platform and the software structure," *Applied Mathematical Modelling*, vol. 53, pp. 693–708, 2018.

[36] C. Liu, G. Luo, Z. Chen, and W. Tu, "Measurement delay compensated LADRC based current controller design for PMSM drives with a simple parameter tuning method," *ISA Transactions*, vol. 101, pp. 482–492, 2020.

[37] D. Sun, "Sensorless control of surface mounted permanent magnet synchronous motor based on improved extended state observer," *Electric Drive*, vol. 51, no. 3, pp. 2–8, 2021.

[38] D. Sun and Y. Zhang, "Improvement and observation accuracy analysis of linear extended state observer," *Journal of National University of Defense Technology*, vol. 39, no. 6, pp. 111–117, 2017.

[39] T. Y. Jeon and B.-G. Jung, "A study of PI controller tuning methods using the internal model control guide for a ship central cooling system as a multi-input single-output system," *Journal of Marine Science and Engineering*, vol. 11, no. 10, 2023.

[40] N. Zeng, Z. Wang, W. Liu, H. Zhang, K. Hone, and X. Liu, "A dynamic neighborhood-based switching particle swarm optimization algorithm," *IEEE Transactions on Cybernetics*, vol. 52, no. 9, pp. 9290–9301, 2022.

[41] W. Liu, Z. Wang, X. Liu, N. Zeng, and D. Bell, "A novel particle swarm optimization approach for patient clustering from emergency departments," *IEEE Transactions on Evolutionary Computation*, vol. 23, no. 4, pp. 632–644, 2019.

[42] W. Liu, Z. Wang, Y. Yuan, N. Zeng, K. Hone, and X. Liu, "A novel sigmoid-function-based adaptive weighted particle swarm optimizer," *IEEE Transactions on Cybernetics*, vol. 51, no. 2, pp. 1085–1093, 2021.

[43] J. Fang, W. Liu, L. Chen, S. Lauria, A. Miron, and X. Liu, "A survey of algorithms, applications and trends for particle swarm optimization," *International Journal of Network Dynamics and Intelligence*, vol. 2, no. 1, pp. 24–50, 2023.

[44] L. Xu, B. Song, and M. Cao, "An improved particle swarm optimization algorithm with adaptive weighted delay velocity," *Systems Science and Control Engineering*, vol. 9, no. 1, pp. 188–197, 2021.

[45] L. Xu, M. Cao, and B. Song, "A new approach to smooth path planning of mobile robot based on quartic Bezier transition curve and improved PSO algorithm," *Neurocomputing*, vol. 473, pp. 98–106, 2022.

[46] X. Wang, Y. Sun, and D. Ding, "Adaptive dynamic programming for networked control systems under communication constraints: a survey of trends and techniques," *International Journal of Network Dynamics and Intelligence*, vol. 1, no. 1, pp. 85–98, 2022.

[47] Z. Lu and G. Guo, "Control and communication scheduling co-design for networked control systems: a survey," *International Journal of Systems Science*, vol. 54, no. 1, pp. 189–203, 2023.

[48] Y. Shen, Z. Wang, H. Dong, and H. Liu, "Multi-sensor multi-rate fusion estimation for networked systems: advances and perspectives," *Information Fusion*, vol. 82, pp. 19–27, 2022.

[49] D. Zhao, Z. Wang, L. Wang, and G. Wei, "Proportional-integral observer design for multirate-networked systems under constrained bit rate: an encoding-decoding mechanism," *IEEE Transactions on Cybernetics*, vol. 53, no. 7, pp. 4280–4291, 2023.